First-principles calculations of spin interactions and the magnetic ground states of Cr trimers on Au(111)

A. Antal,[1] B. Lazarovits,[1,2] L. Udvardi,[1,3] L. Szunyogh,[1] B. Újfalussy,[3] and P. Weinberger[4]
[1]*Department of Theoretical Physics, Budapest University of Technology and Economics, Budafoki út 8, H-1111 Budapest, Hungary*
[2]*Research Institute for Solid State Physics and Optics, Hungarian Academy of Sciences, P.O. Box 49, H-1525 Budapest, Hungary*
[3]*BME-HAS Group of Solid State Physics, Budapest University of Technology and Economics, Budafoki út 8, H-1111 Budapest, Hungary*
[4]*Center for Computational Nanoscience, Seilerstätte 10/22, A-1010 Vienna, Austria*
(Received 29 February 2008; revised manuscript received 30 April 2008; published 23 May 2008)

We present calculations of the magnetic ground states of Cr trimers in different geometries on top of a Au(111) surface. By using a least squares fit method based on results obtained by means of a fully relativistic embedded-cluster Green's function method, first we determined the parameters of a classical spin vector model containing second- and fourth-order interactions. The developed method requires no *a priori* assumed symmetry constraints; therefore, it is applicable throughout for small nanoparticles of arbitrary geometry. The magnetic ground states were then found by solving the Landau-Lifshitz-Gilbert equations. In all cases considered, the configurational energy of the Cr trimers is dominated by large antiferromagnetic nearest neighbor interactions, while the biquadratic spin interactions provide the second largest contributions to the energy. We find that an equilateral Cr trimer exhibits a frustrated 120° Néel type of ground state with a small out-of-plane component of the magnetization. Furthermore, we show that the Dzyaloshinsky-Moriya interactions determine the chirality of the magnetic ground state. In cases of a linear chain and an isosceles trimer, collinear antiferromagnetic ground states are obtained with the magnetization lying parallel to the surface.

DOI: 10.1103/PhysRevB.77.174429 PACS number(s): 75.10.Hk, 75.30.Et, 75.80.+q

I. INTRODUCTION

The development of nanoscale devices based on electron spin requires both a fundamental understanding of magnetic interactions and practical solutions to a variety of challenges. Deposited clusters are of special interest due to their possible applications in miniaturized data storage technology. The development of scanning tunneling microscopy (STM) and the ability to build clusters with well-controlled structures permit the measurement of various effects induced by local interactions within magnetic nanoclusters. Recent STM studies investigated the coupling between the magnetic and electronic degrees of freedom of nanoparticles and the conducting substrate for adatoms,[1–3] dimers,[4,5] and trimers.[6] Very recently, Wahl *et al.*[7] were even able to estimate the exchange coupling between Co adatoms on a Cu(001) surface by probing the Kondo resonance in terms of low temperature scanning tunneling spectroscopy. Obviously, a large number of theoretical efforts were also focused on the description of the Kondo effect of single atoms or small clusters.[8–12]

First-principles studies of supported clusters are extremely useful for a clear interpretation of obtained experimental results and add substantially to the understanding of the underlying physical phenomena. Determining, in general, the noncollinear magnetic ground states of finite nanoparticles on an *ab initio* level is clearly a very demanding task in computational science. One possible alternative is based on a fully unconstrained local spin-density approach (LSDA) implemented via the full-potential linearized augmented plane-wave method[13] or the projector augmented-wave method.[14] However, unconstrained noncollinear calculations have also been performed within the atomic sphere approximation by using a real-space linearized muffin-tin orbital (LMTO) method[15–17] or the Korringa-Kohn-Rostoker (KKR) method.[18] Another approach[19–21] relies on *ab initio* spin dynamics in terms of a constrained LSDA by means of a fully relativistic KKR method solving simultaneously the Landau-Lifshitz-Gilbert (LLG) equations for the evolution of the orientations of spin magnetic moments. Although such simulations are very accurate in finding the magnetic ground state of complex systems, they are very costly and, in practice, require a massively parallel computer architecture.

In past years, it turned out that multiscale approaches based on a first principles evaluation of model parameters are very useful to study both the ground state and the dynamics of spin systems. In Refs. 22–24, the torque method[25] was employed to calculate isotropic exchange interactions, followed by Monte Carlo simulations to study the temperature dependent magnetism of nanoclusters. This approach can, in principle, be extended to include relativistic contributions to the exchange interactions.[26] Nevertheless, because of the low (or even missing) symmetry of nanoparticles, the determination of the exchange coupling and the on-site anisotropy matrices becomes quite complicated. Moreover, as found, e.g., for Mn and Cr monolayers on Cu(111), higher-order spin interactions are needed for an accurate mapping of the energy obtained from first principles calculations.[13] Recently, a fast *ab initio* approach that makes use of a suitable parametrization of the configurational energy of a complex magnetic system, namely, a spin cluster expansion, has been proposed,[27,28] but not yet applied intensively.

In here, we introduce yet another scenario to construct parameters for a classical spin model containing interactions, in principle, up to arbitrary order. Our method is based on relativistic first principles calculations of the energy, whereby a sufficiently large number of states with different noncollinear magnetic configurations (orientational states) are considered to enable a least squares fit of the parameters

of the spin model. In order to determine the magnetic ground state of the system we then solve the Landau-Lifshitz-Gilbert equations that correspond to the assumed classical spin Hamiltonian.

The half-filled valence band configuration of Cr causes a large spin magnetic moment. Furthermore, strong antiferromagnetic interatomic bonding leads to magnetic frustration and complex spin phenomena. The simplest system exhibiting such properties is a trimer. It is worthwhile to mention that the noncollinear magnetic structure of supported triangular clusters has first been investigated by means of a self-consistent vector Anderson model.[29] First-principles calculations revealed a frustrated noncollinear magnetic structure for an equilateral Cr trimer supported on a Au(111) surface[16,30] and, on the other hand, a collinear antiferromagnetic magnetic ground state for a linear chain of three Cr atoms.[16]

We apply our method to Cr trimers deposited on a Au(111) surface in equilateral, linear, and isosceles geometries. Although these systems are governed by large antiferromagnetic nearest neighbor coupling, we will point out the crucial role of the relativistic interactions in the formation of the magnetic ground state. In particular, it will be shown that for an equilateral trimer the Dzyaloshinsky-Moriya interactions determine the chirality of the magnetic ground state; whereas in cases of linear and isosceles trimers, the inter- and on-site anisotropic terms lead to an in-plane orientation of the antiferromagnetic ground state.

II. THEORETICAL APPROACHES AND COMPUTATIONAL METHODS

A. Energy of a classical spin system

Neglecting intra-atomic noncollinearity, the magnetic state of L atoms is described by the array $\{\vec{M}_i\}_{i=1,\ldots,L}$, where $\vec{M}_i = M_i\vec{\sigma}_i$ ($|\vec{\sigma}_i|=1$) is the spin magnetic moment of a particular atom labeled by i. In a large class of magnetic systems, referred to as "good moment" systems, the longitudinal fluctuations of the spin moments can also be neglected; i.e., the magnitudes of the spin moments, M_i, can be considered to be independent of the orientational state $\{\vec{\sigma}_i\}_{i=1,\ldots,L}$. The most general expression of the energy up to second order in the classical spin vectors can be written as

$$E(\{\vec{\sigma}_i\}) = E^{(0)} + E^{(2)}(\{\vec{\sigma}_i\}), \tag{1}$$

with

$$E^{(2)}(\{\vec{\sigma}_i\}) = \frac{1}{2}\sum_{i\neq j}\vec{\sigma}_i\mathbf{J}_{ij}\vec{\sigma}_j + \sum_i \vec{\sigma}_i\mathbf{K}_i\vec{\sigma}_i, \tag{2}$$

where $\mathbf{J}_{ij}=\{J_{ij}^{\alpha\beta}\}$ ($\alpha,\beta=x,y,z$) are generalized exchange interaction matrices and $\mathbf{K}_i=\{K_i^{\alpha\beta}\}$ are the (second-order) on-site anisotropy constant matrices. Within a nonrelativistic approach, the on-site anisotropy constants vanish, just as well as the exchange tensor is of a simple diagonal form, $\mathbf{J}_{ij}=J_{ij}\mathbf{I}$, with $\mathbf{I}$ being the unit matrix. Thus, an isotropic Heisenberg model is recovered. For a transparent physical interpretation of the exchange tensor, $\mathbf{J}_{ij}$ can be decomposed into three terms as[26]

$$\mathbf{J}_{ij} = J_{ij}\mathbf{I} + \mathbf{J}_{ij}^S + \mathbf{J}_{ij}^A, \tag{3}$$

where J_{ij} is the isotropic part of the exchange tensor,

$$J_{ij} = \frac{1}{3}\mathrm{Tr}(\mathbf{J}_{ij}), \tag{4}$$

and the traceless symmetric anisotropic exchange tensor $\mathbf{J}_{ij}^S$ is defined by

$$\mathbf{J}_{ij}^S = \frac{1}{2}(\mathbf{J}_{ij} + \mathbf{J}_{ij}^T) - J_{ij}\mathbf{I}, \tag{5}$$

where T denotes the transpose of a matrix. The antisymmetric exchange matrix $\mathbf{J}_{ij}^A$, is then given by

$$\mathbf{J}_{ij}^A = \frac{1}{2}(\mathbf{J}_{ij} - \mathbf{J}_{ij}^T). \tag{6}$$

The antisymmetric part of the intersite exchange interaction can be cast in the following form:

$$\vec{\sigma}_i\mathbf{J}_{ij}^A\vec{\sigma}_j = \vec{D}_{ij}(\vec{\sigma}_i\times\vec{\sigma}_j), \tag{7}$$

which is nothing but the well-known relativistic Dzyaloshinsky-Moriya (DM) interaction,[31,32] with the vector $\vec{D}_{ij}$ defined as

$$D_{ij}^x = \frac{1}{2}(J_{ij}^{yz} - J_{ij}^{zy}), \quad D_{ij}^y = \frac{1}{2}(J_{ij}^{zx} - J_{ij}^{xz}), \quad D_{ij}^z = \frac{1}{2}(J_{ij}^{xy} - J_{ij}^{yx}). \tag{8}$$

The asymmetric exchange interactions induced by spin-orbit coupling have been shown to have crucial consequences on the magnetic ground state in thin films.[33,34] For transition metal clusters, such effects are expected to be even more important due to reduced rotational symmetry.

Unlike most thin films with uniaxial or biaxial symmetry, in the case of finite clusters, the structure of the on-site anisotropy matrices cannot, in general, be predicted "*a priori*," i.e., from symmetry principles. The on-site anisotropy can, at best, be characterized by diagonalizing the matrix $\mathbf{K}_i$,

$$\vec{\sigma}_i\mathbf{K}_i\vec{\sigma}_i = \sum_\lambda K_i^\lambda(\vec{\sigma}_i\cdot\vec{e}_i^\lambda)^2, \tag{9}$$

where K_i^λ and the unit vectors $\vec{e}_i^\lambda$ ($\lambda=1,2,3$) are the eigenvalues and corresponding eigenvectors of $\mathbf{K}_i$. Clearly, the easy axis is associated by that eigenvector that refers to the minimum value of K_i^λ. Note that the matrix $\mathbf{K}_i$ can be chosen to be symmetric; therefore, the eigenvectors $\vec{e}_i^\lambda$ are pairwise normal to each other. Obviously, the symmetric anisotropic exchange interaction [see Eq. (5)] can be decomposed in a similar way,

$$\vec{\sigma}_i\mathbf{J}_{ij}^S\vec{\sigma}_j = \sum_\lambda J_{ij}^{S,\lambda}(\vec{\sigma}_i\cdot\vec{e}_{ij}^\lambda)(\vec{\sigma}_j\cdot\vec{e}_{ij}^\lambda), \tag{10}$$

with $J_{ij}^{S,\lambda}$ and $\vec{e}_{ij}^\lambda$ being the eigenvalues and eigenvectors of the matrix $\mathbf{J}_{ij}^S$, respectively.

However, the second-order approximation in Eq. (2) is not always sufficient to describe the energy of a magnetic system.[13] As will be shown, adding a further term, $E^{(4)}$, to Eq. (1) corresponding to fourth-order spin interactions con-

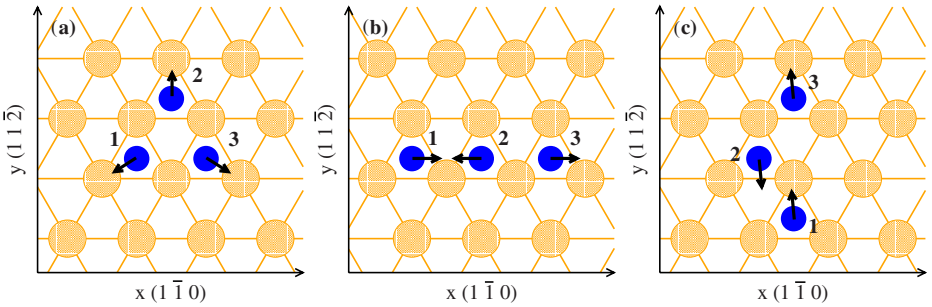

FIG. 1. (Color online) Geometries of the Cr trimers (solid circles) deposited on top of a Au(111) surface (patterned circles): (a) equilateral triangle, (b) linear chain, and (c) isosceles triangle. The arrows denote the ground state orientation of the spin magnetic moments of the Cr atoms.

siderably improves the quality of the mapping of the energy from first principles calculations to the spin model. In order to keep our model tractable, we extended Eq. (1) only by the following rotational invariant fourth-order terms:

$$E^{(4)}(\{\vec{\sigma}_i\}) = \sum_{\substack{i,j,k,l \\ (i<j,k<l)}} Q_{ijkl}(\vec{\sigma}_i \cdot \vec{\sigma}_j)(\vec{\sigma}_k \cdot \vec{\sigma}_l). \tag{11}$$

It is easy to see that in case of three atoms, the above sum consists of only six different terms; therefore, the following simplified notation can be used:

$$Q_{12} = Q_{1212}, \quad Q_{13} = Q_{1313}, \quad Q_{23} = Q_{2323},$$
$$Q^1_{23} = Q_{1213}, \quad Q^2_{13} = Q_{2123}, \quad Q^3_{12} = Q_{3132}.$$

We determined the parameters $J^{\alpha\beta}_{ij}$, $K^{\alpha\beta}_i$, Q_{ij} and Q^i_{jk} for different Cr trimers on a Au(111) surface by fitting the energy of the orientational states obtained from first principles calculations to Eq. (2) augmented by the terms in Eq. (11).

B. Evaluation of the parameters for Cr trimers

In order to calculate the electronic structure of the Cr_3 clusters, we applied the embedded-cluster Green's function technique based on the Korringa-Kohn-Rostoker method (KKR-EC).[35] Within the KKR-EC, the matrix of the so-called scattering path operator (SPO), $\boldsymbol{\tau}_{\mathcal{C}}$, corresponding to a finite cluster $\mathcal{C}$ embedded into a host system can be obtained from the following Dyson equation:

$$\boldsymbol{\tau}_{\mathcal{C}}(E) = \boldsymbol{\tau}_h(E)\{\boldsymbol{I} - [\boldsymbol{t}_h^{-1}(E) - \boldsymbol{t}_{\mathcal{C}}^{-1}(E)]\boldsymbol{\tau}_h(E)\}^{-1}, \tag{12}$$

where $\boldsymbol{t}_h(E)$ and $\boldsymbol{\tau}_h(E)$ denote the single-site scattering matrix and the SPO matrix for the pristine host confined to the sites in $\mathcal{C}$, respectively, while $\boldsymbol{t}_{\mathcal{C}}$ comprises the single-site scattering matrices of the embedded atoms. Note that Eq. (12) accounts for all scattering events in the system merging the cluster and the host. Once $\boldsymbol{\tau}_{\mathcal{C}}$ is derived, all quantities of interest for a cluster, i.e., the charge and magnetization densities and the spin and orbital moments, as well as the exchange interaction energy, can be calculated. The electronic structure of the host gold surface, including three layers of empty spheres to represent the vacuum region, was calculated in terms of the fully relativistic screened Korringa-Kohn-Rostoker method.[36,37] The cluster calculations were then carried out such that the Cr atoms substituted empty spheres on top of the surface making, however, no attempts to include lattice relaxation effects. Figure 1 shows the geometry of the three Cr trimers considered in the present study, namely, an equilateral triangle, a linear chain, and an isosceles triangle.

The local spin-density approximation as parametrized by Vosko *et al.*[38] was applied; the effective potentials and fields were treated within the atomic sphere approximation. When solving the Kohn-Sham-Dirac equation and also for the multipole expansion of the charge densities, we used a cutoff of $\ell_{\max}=2$. When performing self-consistent calculations for the linear chain and the isosceles triangle, we fixed the direction of the magnetization on all the three Cr atoms normal to the surface; while for the equilateral trimer, we used the 120° Néel state indicated by the arrows in Fig. 1(a) as reference (see Sec. III A).

For the calculation of the energy of the orientational states, we applied the magnetic force theorem[39–43] by using the self-consistent potentials determined for the above mentioned reference states. In using this theorem, only band-energy differences have to be calculated requiring, however, highly precise Brillouin zone integrals.[35] For this purpose, $\boldsymbol{\tau}_h(E)$ was evaluated using over 3300 k points in the irreducible (1/6) segment of the surface Brillouin zone.

In order to determine the parameters of our spin model, we generated a large number of random magnetic configurations $\{\vec{\sigma}^n_i\}$, where $n=1,\ldots,N$, and calculated the corresponding band energies[35] $E^n_b=E_b(\vec{\sigma}^n_1,\vec{\sigma}^n_2,\vec{\sigma}^n_3)$. Introducing an ordered (row) vector containing all combinations of the components of $\vec{\sigma}^n_{i,\alpha}$ $(\alpha=x,y,z)$ occurring in Eqs. (2) and (11),

$$\mathbf{X}^n = \Big(\sigma^n_{1,x}\sigma^n_{2,x}, \sigma^n_{1,x}\sigma^n_{2,y}, \sigma^n_{1,x}\sigma^n_{2,z}, \ldots, \sigma^n_{1,x}\sigma^n_{1,x}, \ldots, \sum_{i,j=x,y,z} \sigma^n_{3,i}\sigma^n_{1,i}\sigma^n_{3,j}\sigma^n_{2,j}\Big), \tag{13}$$

and a vector of the corresponding parameters of the fourth-order spin model,

$$\mathbf{P} = (J^{xx}_{12}, J^{xy}_{12}, J^{xz}_{12}, \ldots, K^{xx}_1, \ldots, Q^3_{12}), \tag{14}$$

the energy of the nth configuration can simply be written as

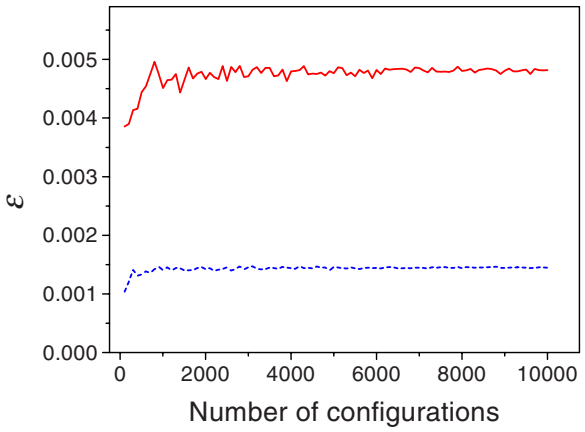

FIG. 2. (Color online) The evolution of the relative error $\varepsilon = \sqrt{\Delta E^2/\langle E^2\rangle}$ of the fitting procedure against the number of considered configurations for the isosceles Cr trimer. The solid (red) and the dashed (blue) lines refer to the parameter set excluding and including rotational invariant biquadratic terms in the spin model, respectively.

$$E^n = \mathbf{P}(\mathbf{X}^n)^T. \tag{15}$$

An optimal choice of the parameters is to minimize the difference (error) between the calculated band energies E_b^n and the energy related to the spin model, E^n. The square of this error is defined as

$$\Delta E^2 = \sum_{n=1}^{N} (E^n - E_b^n)^2, \tag{16}$$

and substituting Eq. (15) in a least squares condition leads to the solution

$$\mathbf{P} = \sum_n E_b^n \mathbf{X}^n \left[\sum_n (\mathbf{X}^n)^T \mathbf{X}^n \right]^{-1}. \tag{17}$$

The number of considered random configurations can be increased until the parameters are converged.

The quality of the fit is characterized by the relative error $\varepsilon = \sqrt{\Delta E^2/\langle E^2\rangle}$, where $\langle E^2\rangle$ is the average of $(E_b^n)^2$ over all the configurations. This relative error as a function of the number of configurations, N, is of very similar shape for all the three clusters. As it is shown in Fig. 2, for a Cr trimer forming an isosceles triangle, the error of the fit stabilizes around 0.48% above $N \simeq 5000$ when using only the second-order spin interactions; see Eq. (2). The error, however, is reduced to 0.14%, including the fourth-order terms in Eq. (11). In this case, only about 2000 configurations were sufficient to obtain a stable error.

The configurational energy of the Cr trimers is dominated by quite large antiferromagnetic isotropic exchange interactions, $J_{ij} \simeq 100-150$ meV. In general, we obtained DM interactions smaller by 2 orders of magnitude, $D_{ij} \simeq 0.5-2.0$ meV; whereas the typical range of the anisotropic symmetric exchange interactions and the on-site anisotropy constants was about 0.1 meV or even less. This trend can be understood in terms of a perturbational treatment with respect to the spin-orbit coupling parameter ξ since the DM interactions turn to be proportional to ξ, whereas the anisotropy terms appear (at best) in a second-order expansion in ξ. Obviously, a required relative accuracy for the small interaction parameters can be achieved only with a number of configurations much larger than that used for the total configurational energy. This is demonstrated in Fig. 3, showing the evolution of the DM interactions for an isosceles Cr trimer. As can be inferred from this figure, about 7000 configurations are needed to stabilize the values of the D_{ij} within a relative accuracy of 1%. In order to achieve the same relative accuracy for the coefficients with the smallest magnitude, namely, for the in-plane on-site anisotropy constants, we had to generate about 10000 random configurations.

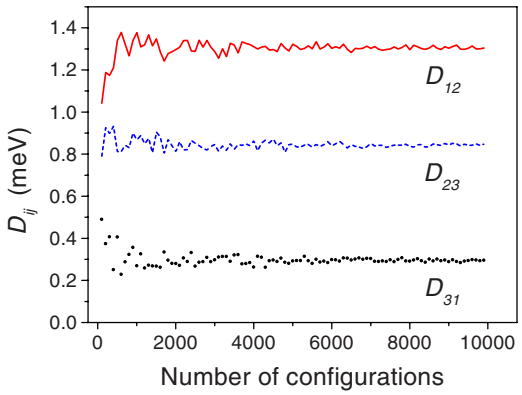

FIG. 3. (Color online) Convergence of the magnitudes of the Dzyaloshinsky-Moriya vectors, D_{ij}, versus the number of configurations for the case of an isosceles Cr trimer. The labels of the DM vectors refer to the numbering of Cr atoms in Fig. 1(c).

C. Determination of the magnetic ground state

Once the parameters of the spin model are fixed, the ground state configuration of the system can easily be determined by solving the Landau-Lifshitz-Gilbert equations for the transversal components of the magnetizations,

$$\frac{\partial \vec{\sigma}_i}{\partial t} = -\frac{\gamma}{1+\alpha^2}\vec{\sigma}_i \times \vec{H}_i^{\text{eff}} - \frac{\alpha\gamma}{1+\alpha^2}\vec{\sigma}_i \times (\vec{\sigma}_i \times \vec{H}_i^{\text{eff}}), \tag{18}$$

where γ and α are the gyromagnetic ratio and the Gilbert damping factor, respectively, and the effective fields $\vec{H}_i^{\text{eff}}$ are defined by

$$\vec{H}_i^{\text{eff}} = -\frac{1}{M_i}\frac{\partial E(\{\vec{\sigma}\})}{\partial \vec{\sigma}_i}, \tag{19}$$

as follows from using Eqs. (2) and (11). It should be stressed that in the present context, Eq. (18) is merely used as a numerical tool to find efficiently the energy minimum, describing the noncollinear configurations of the Cr trimers. In all cases, we started the simulations at randomly chosen arbitrary configurations. The stability and the speed of the applied numerical procedure, a fourth-order Runge-Kutta method, for integrating Eq. (18) was, therefore, optimized by adjusting the phenomenological parameters γ and α. As we checked, however, the magnetic ground state we found by

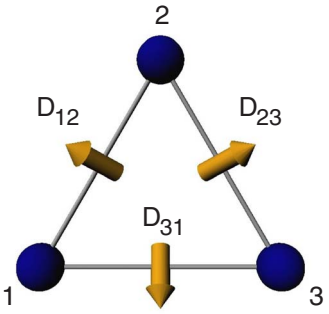

FIG. 4. (Color online) Schematic view of the DM vectors for an equilateral Cr trimer.

solving the LLG equations was always independent on the choice of γ and α.

III. RESULTS AND DISCUSSIONS

A. Equilateral trimer

We first investigated a Cr trimer forming an equilateral triangle on top of Au(111), as shown in Fig. 1(a). Since our previous first principles spin-dynamics calculations[21] resulted in a 120° Néel type of ground state [see Fig. 1(a)], in here we used this configuration as a reference state to determine the effective potentials and exchange fields self-consistently. Reassuringly, the calculated spin magnetic moments of the Cr atoms, 4.4 μ_B, proved to be practically independent of the magnetic configuration of the trimer. Furthermore, our calculations yielded very small orbital magnetic moments, ~0.03 μ_B, as a consequence of the nearly half band filling of Cr. Since in this case both the substrate and the trimer exhibit a c_{3v} point-group symmetry, the exchange interaction matrices $\mathbf{J}_{12}$, $\mathbf{J}_{13}$, and $\mathbf{J}_{23}$, as well as the on-site anisotropy matrices $\mathbf{K}_1$, $\mathbf{K}_2$, and $\mathbf{K}_3$, are related in terms of appropriate similarity transformations. The number of independent parameters of the model is therefore considerably reduced; e.g., the isotropic exchange parameters become identical and the on-site anisotropy matrix corresponding to the atom labeled 2 in Fig. 1(a) is of the form

$$\mathbf{K}_2 = \begin{bmatrix} K_2^{xx} & 0 & 0 \\ 0 & K_2^{yy} & K_2^{yz} \\ 0 & K_2^{yz} & K_2^{zz} \end{bmatrix}. \tag{20}$$

As a consistency check of our fitting process, the obtained parameters satisfied all symmetries inherent to this system.

The dominant parameters determining the ground state of this Cr trimer are the isotropic exchange interactions $J_{12}=J_{13}=J_{23}=144.9$ meV and the DM interactions with magnitudes $D_{12}=D_{13}=D_{23}=1.78$ meV. As mentioned earlier, the on-site anisotropy terms are much smaller in magnitude, e.g., $K_2^{xx}=-0.09$ meV in Eq. (20). As indicated in Fig. 4, the lines of the DM vectors cross each other at a common point lying on the c_{3v} symmetry axis of the Cr trimer. This is a consequence of Moriya's second rule for the DM vectors;[32] namely, if a mirror plane bisects an edge between a pair of sites then the respective DM vector lies in the mirror plane.

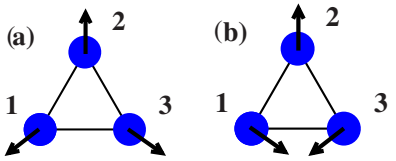

FIG. 5. (Color online) Two typical ground state configurations of an equilateral Cr trimer in the absence of DM interactions. The two configurations refer to different chiralities: (a) $\kappa_z=-1$ and (b) $\kappa_z=1$; see Eq. (21).

Also noteworthy are the coefficients of the biquadratic spin interactions, which are as follows: $Q_{12}=Q_{13}=Q_{23}=-4.42$ meV and $Q_{23}^1=Q_{13}^2=Q_{12}^3=7.06$ meV.

By solving the LLG equations as described in Sec. II C with the above parameters, we indeed obtained the ground state indicated in Fig. 1(a), namely, a state which is very close to an in-plane 120° Néel state with almost negligible out-of-plane components of the spin magnetic moments. Quite obviously, an equivalent ground state can be generated from this state by simultaneously reversing the directions of all the spin magnetic moments.

Considering only isotropic exchange interactions, a frustration induced by the geometry of the Cr trimer leads to an eightfold degenerate noncollinear ground state. These states can be divided into two classes, as indicated in Fig. 5. One class consists of the configuration depicted in Fig. 5(a) and the corresponding one with reversed directions (two configurations); the second class consists of that in Fig. 5(b) and those generated from this state via c_{3v} symmetry transformations and time reversal (six configurations in total). Defining the chirality vector of the system as

$$\vec{\kappa} = \frac{2}{3\sqrt{3}} \sum_{(ij)} (\vec{\sigma}_i \times \vec{\sigma}_j), \tag{21}$$

where the summation runs over the three directed bonds (12, 23, and 31) forming the triangle, the two classes can be assigned to the chiralities $\kappa_z=-1$ and $\kappa_z=1$, respectively. Note that for in-plane configurations, the vector $\vec{\kappa}$ is normal to the plane of the triangle.

Recalling Eq. (7), when switching on the DM interactions, the degeneracy of the ground state is evidently lifted according to the chirality κ_z. In the present case of an in-plane magnetization, the contribution of the DM interaction to the energy can simply be expressed as

$$E_{\mathrm{DM}} = \frac{3\sqrt{3}}{2} D_z \kappa_z, \tag{22}$$

where D_z denotes the z component of any DM vector. Since according to our calculations $D_z=0.97$ meV, the states with $\kappa_z=-1$ depicted in Fig. 5(a) become the ground state of the system, while states with $\kappa_z=1$ [see Fig. 5(b)] are higher in energy by $\Delta E=5.04$ meV. Thus, the ground state we found by solving the LLG equations is caused by the antiferromagnetic exchange interactions and the DM interactions shown in Fig. 4.

Finally in this section, a note has to be added concerning the reference state for the fitting procedure described in Sec.

TABLE I. Calculated isotropic exchange coupling parameters J_{ij}, symmetric anisotropic exchange tensors $\mathbf{J}_{ij}^{S}$, DM vectors $\vec{D}_{ij}$, on-site anisotropy matrices $\mathbf{K}_i$, and biquadratic coupling parameters Q_{ij} and Q_{ij}^{k} for a linear Cr trimer. All data are given in units of meV.

J_{12}		$\mathbf{J}_{12}^{S}$		$\vec{D}_{21}$		$\mathbf{K}_1$	
	0.157	−0.006	−0.014	0.056	−0.092	−0.007	−0.128
99.59	−0.006	0.005	0.063	0.487	−0.007	−0.141	0.013
	−0.014	0.063	−0.162	−0.578	−0.128	0.013	0.233
J_{13}		$\mathbf{J}_{13}^{S}$		$\vec{D}_{31}$		$\mathbf{K}_2$	
	0.022	0.000	0.000	0.000	0.018	0.000	0.000
−17.85	0.000	0.009	0.000	−0.262	0.000	−0.066	0.034
	0.000	0.000	−0.031	0.068	0.000	0.034	0.048
J_{23}		$\mathbf{J}_{23}^{S}$		$\vec{D}_{23}$		$\mathbf{K}_3$	
	0.157	0.006	0.014	0.056	−0.092	0.007	0.128
99.59	0.006	0.005	0.063	−0.487	0.007	−0.141	0.013
	0.014	0.063	−0.162	0.578	0.128	0.013	0.233
Q_{12}	Q_{23}	Q_{13}	Q_{23}^{1}	Q_{13}^{2}		Q_{12}^{3}	
−0.078	−0.078	0.063	−2.449	5.810		−2.449	

II B. As discussed in quite some details in Ref. 21, when choosing a normal-to-plane ferromagnetic reference state, an erroneous ground state [Fig. 5(b)] was obtained. The very reason of this result is that in this case the orientations of the fitted DM vectors differ from those depicted in Fig. 4, namely, yielding $D_z<0$. Clearly from Eq. (22), the energy of the states related to $\kappa_z=1$ are lowered with respect to those related to $\kappa_z=-1$. This observation clearly indicates that for systems with metastable states close to the ground state, one has to be very careful when choosing the reference state serving as basis for subsequent magnetic force theorem calculations.

B. Linear trimer

A linear chain of three Cr atoms on top of a Au(111) surface has been assumed to be of the geometry shown in Fig. 1(b). As can be seen from this figure, this system has only a mirror plane normal to the surface, bisecting the chain. The calculated spin magnetic moments are only slightly different from those for the equilateral triangle: $4.45\mu_B$ at the edges of the chain and $4.47\mu_B$ at the central atom. Quite clearly from Table I, the mirror symmetry imposes certain consequences for the parameters, e.g., $J_{12}=J_{23}$, or $\mathbf{J}_{13}^{S}$ has only diagonal elements, etc. Similar to the equilateral trimer, there are large antiferromagnetic isotropic exchange interactions between the nearest neighbors, while the edge atoms are coupled ferromagnetically. The magnitudes of the nearest neighbor exchange interactions are very similar to those obtained in terms of a real-space LMTO method for Cr dimers.[16] Also in this case, quite large biquadratic terms of type Q_{ij}^{k} were needed to obtain a sufficiently good fit of the band energy.

Although the interactions of relativistic origin contribute only little to the energy, it is instructive to discuss them in some detail. The DM vectors shown schematically in Fig. 6 reflect the underlying covering symmetry of the system: $\vec{D}_{13}$ lies in the mirror plane, while $\vec{D}_{21}$ and $\vec{D}_{23}$, being axial vectors, are mirror images of each other. As in the case of the equilateral triangle, the on-site anisotropy terms and the symmetric anisotropic exchange interactions provide the smallest contributions to the energy. The on-site anisotropy matrix related to site 2 is of the form shown in Eq. (20), whereas no such regularity applies to the matrix elements $\mathbf{K}_1$ and $\mathbf{K}_3$ except that they are related to each other via reflection: $x'=-x$, $y'=y$, and $z'=z$.

As expected just by considering isotropic exchange interactions, the solution of the LLG equation led to an antiferromagnetic ground state; see Fig. 1(b). The direction of the spin magnetic moments are parallel to the $(1\bar{1}0)$ axes, which is consistent with symmetry considerations; namely, that the easy axis of a collinear magnetic system with a mirror plane should lie either parallel or normal to the mirror plane.[20] It is important to note that the ambiguity of the reference state mentioned in Sec. III A does not effect the ground state of the linear chain since the DM interactions evidently vanish in a collinear magnetic state.

C. Isosceles trimer

The third type of Cr trimer we considered is an isosceles triangle, depicted in Fig. 1(c). Apparently, such a trimer has a

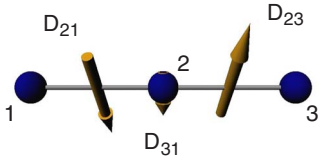

FIG. 6. (Color online) Schematic view of the DM vectors for the linear Cr trimer.

TABLE II. The same as Table I but for the isosceles triangle.

J_{12}		$\mathbf{J}_{12}^{S}$		$\vec{D}_{21}$		$\mathbf{K}_1$	
	−0.126	0.058	0.047	−0.238	−0.091	−0.004	−0.009
117.97	0.058	−0.035	−0.022	−0.472	−0.004	−0.042	−0.029
	0.047	−0.022	0.161	0.656	−0.009	−0.029	0.133
J_{13}		$\mathbf{J}_{13}^{S}$		$\vec{D}_{31}$		$\mathbf{K}_2$	
	−0.019	−0.015	0.019	0.075	−0.120	−0.023	−0.018
−5.60	−0.015	−0.089	−0.025	0.150	−0.023	−0.062	−0.006
	0.019	−0.025	0.109	0.242	−0.018	−0.006	0.181
J_{23}		$\mathbf{J}_{23}^{S}$		$\vec{D}_{23}$		$\mathbf{K}_3$	
	−0.122	−0.094	−0.058	0.610	−0.084	0.024	0.035
117.47	−0.094	0.032	−0.039	−0.335	0.024	−0.069	0.006
	−0.058	−0.039	0.090	1.107	0.035	0.006	0.153
Q_{12}	Q_{23}	Q_{13}	Q_{23}^{1}	Q_{13}^{2}		Q_{12}^{3}	
1.227	1.555	0.271	−0.640	3.966		−0.080	

single mirror plane which, however, does not coincide with those of the surface layer. Therefore, the system possesses no point-group symmetry. Our calculations resulted in spin magnetic moments of $4.45\mu_B$ for the Cr atoms 1 and 3 and $4.46\mu_B$ for Cr atom 2. As can be inferred from Table II, the nearest neighbor isotropic exchange interactions are almost symmetric, $J_{12} \simeq J_{23}$, and the second nearest neighbor isotropic exchange interaction is weakly ferromagnetic. The above data indicate that, similar to many transition metal systems, the formation of local spin moments depends mainly on the nearest neighbor environment of the atoms rather than on long-range interactions or the symmetry of the system.

The second largest contribution to the energy, namely, the biquadratic interactions, clearly reflect the absence of mirror plane since $Q_{12} \neq Q_{23}$ and $Q_{23}^{1} \neq Q_{12}^{3}$. This asymmetry is more striking in the case of the DM vectors; see also Fig. 7. The good convergence of the parameters with respect to the number of configurations seen in Fig. 3 indicates that the large asymmetry of the DM vectors indeed stems from a lack of covering symmetry and not from an error in the fitting procedure. The obtained antiferromagnetic ground state is very similar to that of the linear chain (see Fig. 1); however, the direction of the spin moments is now slightly out of the line connecting sites 1 and 3.

IV. SUMMARY AND CONCLUSIONS

We developed a method in order to map the energy of supported magnetic nanoparticles obtained from first principles calculations onto a classical spin Hamiltonian. As a first application, we determined the spin interactions for three different Cr trimers deposited on a Au(111) surface. We first calculated the electronic structure of the Cr trimers by means of a fully relativistic Green's function embedding method, from which we obtained the spin magnetic moments of the Cr atoms, in very good agreement with x-ray magnetic circular dichroism measurements[44] and with other first principles calculations.[16,17] The relativistic treatment of the electronic structure was inevitably necessary to properly account for spin-orbit coupling, which in turn gives rise to tensorial exchange interactions and magnetic anisotropies influencing the formation of noncollinear ground states, as shown in case of the equilateral trimer.

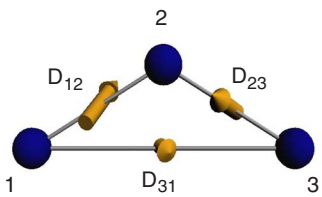

FIG. 7. (Color online) Schematic view of the DM vectors for the isosceles Cr trimer.

In terms of a least squares fit procedure, the most general second-order spin interactions as well as fourth-order terms were then fitted, serving the best approximation to the energies of a large number of random magnetic configurations of the trimers. We have shown that the inclusion of fourth-order terms into the spin model largely enhanced the accuracy of the mapping. A particular advantage of the least squares fit applied in this work is that it is universally applicable as it does not rely on any symmetry restrictions on the model. Moreover, the spin Hamiltonian can, in principle, be extended to an arbitrary order of the spin interactions.

The magnetic ground state of the trimers were found as the solution of the Landau-Lifshitz-Gilbert equations. In the case of an equilateral Cr trimer, we found that the DM interactions lifted the degeneracy of the 120° Néel states with different chirality. On the contrary, for the linear and the isosceles Cr trimers we obtained collinear antiferromagnetic ground states. An issue of choosing the reference state inherent to methods based on the magnetic force theorem was, however, addressed in context with the equilateral Cr trimer. This freedom might cause an ambiguity in determining the magnetic ground state of systems exhibiting metastable states close to the ground state. To overcome this problem, we proposed to use the "true" ground state obtained from

ab initio spin-dynamics calculations[21] as reference since the corresponding spin model proved to be consistent with the "parent" ground state.

The present method can be regarded as a very accurate tool in finding the magnetic ground state of small supported clusters, providing also a clear insight into the role of different interactions in terms of a classical spin model for the formation of the magnetic ground state. As a prospect for the future, the LLG equations will be used to study low-energy spin excitations of nanoparticles; the method introduced here can even be extended to include thermal spin fluctuations.[45,46]

ACKNOWLEDGMENTS

The authors thank G. Zaránd for fruitful discussions. Financial support was provided by the Hungarian National Scientific Research Foundation (Contracts No. OTKA T068312, No. F68726, and No. NF061726).

[1] V. Madhavan, W. Chen, T. Jamneala, M. F. Crommie, and N. S. Wingreen, Science **280**, 567 (1998).
[2] H. C. Manoharan, C. P. Lutz, and D. W. Eigler, Nature (London) **403**, 512 (2000).
[3] T. Jamneala, V. Madhavan, W. Chen, and M. F. Crommie, Phys. Rev. B **61**, 9990 (2000).
[4] W. Chen, T. Jamneala, V. Madhavan, and M. F. Crommie, Phys. Rev. B **60**, R8529 (1999).
[5] V. Madhavan, T. Jamneala, K. Nagaoka, W. Chen, J.-L. Li, S. G. Louie, and M. F. Crommie, Phys. Rev. B **66**, 212411 (2002).
[6] T. Jamneala, V. Madhavan, and M. F. Crommie, Phys. Rev. Lett. **87**, 256804 (2001).
[7] P. Wahl, P. Simon, L. Diekhöner, V. S. Stepanyuk, P. Bruno, M. A. Schneider, and K. Kern, Phys. Rev. Lett. **98**, 056601 (2007).
[8] Yu. B. Kudasov and V. M. Uzdin, Phys. Rev. Lett. **89**, 276802 (2002).
[9] V. V. Savkin, A. N. Rubtsov, M. I. Katsnelson, and A. I. Lichtenstein, Phys. Rev. Lett. **94**, 026402 (2005).
[10] B. Lazarovits, P. Simon, G. Zaránd, and L. Szunyogh, Phys. Rev. Lett. **95**, 077202 (2005).
[11] K. Ingersent, A. W. W. Ludwig, and I. Affleck, Phys. Rev. Lett. **95**, 257204 (2005).
[12] A. A. Aligia, Phys. Rev. Lett. **96**, 096804 (2006).
[13] Ph. Kurz, G. Bihlmayer, K. Hirai, and S. Blügel, Phys. Rev. Lett. **86**, 1106 (2001).
[14] D. Hobbs, G. Kresse, and J. Hafner, Phys. Rev. B **62**, 11556 (2000).
[15] R. Robles and L. Nordström, Phys. Rev. B **74**, 094403 (2006).
[16] A. Bergman, L. Nordström, A. B. Klautau, S. Frota-Pessŏa, and O. Eriksson, J. Phys.: Condens. Matter **19**, 156226 (2007).
[17] A. Bergman, L. Nordstrom, A. Burlamaqui Klautau, S. Frota-Pessŏa, and O. Eriksson, Phys. Rev. B **75**, 224425 (2007).
[18] B. Y. Yavorsky and I. Mertig, Phys. Rev. B **74**, 174402 (2006).
[19] B. Újfalussy, B. Lazarovits, L. Szunyogh, G. M. Stocks, and P. Weinberger, Phys. Rev. B **70**, 100404(R) (2004).
[20] B. Lazarovits, B. Újfalussy, L. Szunyogh, G. M. Stocks, and P. Weinberger, J. Phys.: Condens. Matter **16**, S5833 (2004).
[21] G. M. Stocks, M. Eisenbach, B. Újfalussy, B. Lazarovits, L. Szunyogh, and P. Weinberger, Prog. Mater. Sci. **52**, 371 (2007).
[22] S. Polesya, O. Šipr, S. Bornemann, J. Minár, and H. Ebert, Europhys. Lett. **74**, 1074 (2006).
[23] O. Šipr, S. Bornemann, J. Minár, S. Polesya, V. Popescu, A. Šimunek, and H. Ebert, J. Phys.: Condens. Matter **19**, 096203 (2007).
[24] O. Šipr, S. Polesya, J. Minár, and H. Ebert, J. Phys.: Condens. Matter **19**, 446205 (2007).
[25] A. I. Liechtenstein, M. I. Katsnelson, V. P. Antropov, and V. A. Gubanov, J. Magn. Magn. Mater. **67**, 65 (1987).
[26] L. Udvardi, L. Szunyogh, K. Palotás, and P. Weinberger, Phys. Rev. B **68**, 104436 (2003).
[27] R. Drautz and M. Fähnle, Phys. Rev. B **69**, 104404 (2004); **72**, 212405 (2005).
[28] M. Fähnle, R. Drautz, R. Singer, D. Steiauf, and D. V. Berkov, Comput. Mater. Sci. **32**, 118 (2005).
[29] S. Uzdin, V. Uzdin, and C. Demangeat, Europhys. Lett. **47**, 556 (1999); S. Uzdin, V. Uzdin, and C. Demangeat Comput. Mater. Sci. **17**, 441 (2000); S. Uzdin, V. Uzdin, and C. Demangeat, Surf. Sci. **482-485**, 965 (2001).
[30] H. J. Gotsis, N. Kioussis, and D. A. Papaconstantopoulos, Phys. Rev. B **73**, 014436 (2006).
[31] I. Dzyaloshinsky, J. Phys. Chem. Solids **4**, 241 (1958).
[32] T. Moriya, Phys. Rev. **120**, 91 (1960).
[33] M. Bode, M. Heide, K. von Bergmann, P. Ferriani, S. Heinze, G. Bihlmayer, A. Kubetzka, O. Pietzsch, S. Blügel, and R. Wiesendanger, Nature (London) **447**, 190 (2007).
[34] L. Udvardi, A. Antal, L. Szunyogh, Á. Buruzs, and P. Weinberger, Physica B (Amsterdam) **403**, 402 (2008).
[35] B. Lazarovits, L. Szunyogh, and P. Weinberger, Phys. Rev. B **65**, 104441 (2002).
[36] L. Szunyogh, B. Újfalussy, P. Weinberger, and J. Kollár, Phys. Rev. B **49**, 2721 (1994).
[37] L. Szunyogh, B. Újfalussy, P. Weinberger, and J. Kollár, J. Phys.: Condens. Matter **6**, 3301 (1994).
[38] S. H. Vosko, L. Wilk, and M. Nusair, Can. J. Phys. **58**, 1200 (1980).
[39] G. H. O. Daalderop, P. J. Kelly, and M. F. H. Schuurmans, Phys. Rev. B **41**, 11919 (1990).
[40] L. Szunyogh, B. Újfalussy, and P. Weinberger, Phys. Rev. B **51**, 9552 (1995).
[41] H. J. F. Jansen, Phys. Rev. B **59**, 4699 (1999).
[42] B. Lazarovits, L. Szunyogh, and P. Weinberger, Phys. Rev. B **67**, 024415 (2003).
[43] B. Újfalussy, L. Szunyogh, and P. Weinberger, Phys. Rev. B **54**, 9883 (1996).
[44] P. Ohresser, H. Bulou, S. S. Dhesi, C. Boeglin, B. Lazarovits, E. Gaudry, I. Chado, J. Faerber, and F. Scheurer, Phys. Rev. Lett. **95**, 195901 (2005).
[45] V. P. Antropov, M. I. Katsnelson, B. N. Harmon, M. van Schilfgaarde, and D. Kusnezov, Phys. Rev. B **54**, 1019 (1996).
[46] O. Eriksson, Lecture on International Conference on Computational Materials Science, Cocoyoc, Mexico, 4–8 Feb. 2008 (unpublished).